

Low-density molecular gas of tightly-bound Rashba-Dresselhaus fermions

So Takei,¹ Chien-Hung Lin,¹ Brandon M. Anderson,² and Victor Galitski^{1,3}

¹*Condensed Matter Theory Center, Department of Physics,
The University of Maryland College Park, MD, 20742, USA*

²*National Institute for Standards and Technology, Gaithersburg, MD, 20899, USA*

³*Joint Quantum Institute, Department of Physics,
The University of Maryland College Park, MD, 20742, USA*

(Dated: September 26, 2021)

We study interacting Rashba-Dresselhaus fermions in two spatial dimensions. First, we present a new exact solution to the two-particle pairing problem of spin-orbit-coupled fermions for arbitrary Rashba and Dresselhaus spin-orbit interactions. An exact molecular wave function and the Green function are explicitly derived along with the binding energy and the spectrum of the molecular state. In the second part, we consider a thermal Boltzmann gas of fermionic molecules and compute the time-of-flight velocity and spin distributions for a single fermion in the gas. We show that the pairing signatures can be observed already in the first-moment expectation values, such as time-of-flight density and spin profiles.

PACS numbers:

I. INTRODUCTION

The concept of bound states of fermion pairs arises ubiquitously in physics. The interior of a neutron star is believed to be a superfluid of bound neutron pairs held together by an attractive component of the inter-nucleon interactions.¹ In particle physics, mesons are a bound state of two fermions, a quark and an anti-quark, with the attraction provided by the strong interaction. Arguably the most well-known two-fermion bound state in condensed matter physics is the Cooper pair², bound together in some cases through phonon exchange³, which is the key component in the understanding of superconductivity.

A bound state of a fermion pair also plays an important role in the field of ultracold gases of neutral Fermi atoms, where atoms in two different hyperfine states can be used to realize pairing. With the advent of the Feshbach resonance⁵⁻⁹ experimentalists are now able to adjust both the magnitude and sign of the two-body scattering length by simply tuning an external magnetic field¹⁰⁻¹⁴. This has opened doors to a new field which explores the crossover between a BCS superfluid of weakly bound Cooper pairs and a Bose-Einstein condensate (BEC) of tightly bound fermionic molecules.¹⁵⁻¹⁸ The BEC of such molecules have been observed in time-of-flight (TOF) experiments which show a characteristic bimodal distribution similar to the one observed in a BEC of bosonic atoms.¹⁹⁻²³

In addition to the unprecedented control over the strength and nature of inter-atomic interactions experimentalists are also capable of fine-tuning with relative ease the structures and parameters of these atomic systems using quantum optical techniques. These developments open the possibility of emulating various solid state systems using ultra-cold atomic systems, and using them to gain insights into the outstanding problems in strongly correlated condensed matter physics.^{4,24,25} In

this regard, the theoretical proposals²⁶⁻³¹ for generating synthetic Abelian and non-Abelian gauge fields for a gas of neutral fermionic atoms, and the recent experimental realization of the phenomenon by the NIST group³²⁻³⁴, brings great excitement to the community. While a spatially inhomogeneous Abelian gauge field can mimic the role of an external magnetic field, a uniform non-Abelian gauge field is capable of introducing spin-orbit (SO) interactions akin to Rashba and Dresselhaus couplings found in semiconductor electronic systems.³⁰ These achievements may serve as a key ingredient when realizing some of the most intriguing phases of matter in condensed matter physics, including fractional quantum Hall liquids^{35,36} and topological insulators^{37,38}.

A fundamental feature of low-density electronic systems with Rashba SO interaction is the enhanced tendency for bound pair formation due to a SO-induced increase in the density of states of low-energy electrons.³⁹ An inspection of the single-particle energy spectrum for a Rashba particle reveals a ring of minima in energy in contrast to a single minimum at the momentum-space origin for a particle without SO coupling. Indeed, it has been noted, for instance, that SO interaction can be remarkably beneficial for superconducting pairing.⁴⁰ The experimental realization of SO interactions in ultracold Fermi gases has motivated many recent theoretical works.⁴¹ Some of these include the BCS-BEC crossover physics⁴²⁻⁴⁶ and the effects of population imbalance and superfluidity⁴⁷⁻⁵² in the presence of SO interactions, as well as properties of the BEC ground state in the strong gauge-field limit⁵³.

In this work, we study tightly-bound molecules of Rashba-Dresselhaus fermions in two spatial dimensions, and investigate the properties of a low-density thermal gas of such molecules. We first develop in detail the exact solution to the problem of two Rashba-Dresselhaus fermions interacting via an attractive short-ranged s -wave interaction. The wave function for the bound

molecular state is then obtained by solving for the bound state energy and the molecular energy spectrum. We then focus on a low-density Boltzmann gas of these bound molecules and compute the *single-fermion* density matrix for one of the two fermions that form a molecule in the gas. With this density matrix we evaluate the fermion velocity and spin density distributions in momentum space that can be inferred from a TOF experiment. We compare and contrast these distributions with those corresponding to a non-interacting Boltzmann gas of SO-coupled fermions. The main finding that stems from this consideration is that the pairing of a fermion with its molecular partner has an experimentally observable imprint on these distributions, and that these imprints are absent when fermions are not interacting. We show that these signatures of pairing appear already, for instance, in the first-moment density expectation value $\langle n(\mathbf{k}) \rangle$. Higher-order correlations as a means to probe many-body states has previously been proposed in the context of ultra-cold atoms.⁵⁴

The paper is organized as follows. The exact solution to the above-mentioned interacting two-particle problem is presented in Sec. II. The properties of the bound molecular state are explored in Sec. III: analytic expressions for the binding energy and the molecular spectrum in different physical limits are shown in Secs. III A and III B, respectively. Effects due to a Zeeman term is briefly discussed in Sec. III C. In Sec. IV, we consider a thermal gas of non-interacting molecules and focus on the single-fermion density matrix for such a system (Sec. IV B). There, we compute the TOF velocity (Sec. IV C) and spin (IV D) distributions for a single fermion in the system. In Sec. IV E we discuss how these distributions can be measured experimentally.

II. THE EXACT TWO-PARTICLE WAVE FUNCTION

Let us begin with a system of two “spin”-1/2 fermions with two-dimensional Rashba and Dresselhaus SO interactions moving in two spatial dimensions. The single-particle Hamiltonian is given by

$$\hat{H}_{RD}(\mathbf{k}) = \epsilon_{\mathbf{k}} \hat{\mathbb{I}} + \alpha (\hat{\sigma}_x k_y - \hat{\sigma}_y k_x) + \beta (\hat{\sigma}_x k_x - \hat{\sigma}_y k_y), \quad (1)$$

where $\epsilon_{\mathbf{k}} = k^2/2m$ with m being the mass of the particle, $\hat{\sigma} = (\hat{\sigma}_x, \hat{\sigma}_y)$ are the usual Pauli matrices and $\mathbf{k} = (k_x, k_y)$ is the particle momentum. We will be using units where $\hbar = 1$ throughout. The term proportional to α (β) is known as the Rashba (Dresselhaus) SO interaction. The hats denote 2×2 matrices acting on the “spin”-space of the particle. Here, the “spin” degree of freedom may be a *synthetic* degree of freedom. Hamiltonian (1), for instance, can be realized in ultra-cold atomic systems where atoms with multiple internal levels move in the presence of a spatially modulated laser field.^{30,63}

For the two-particle system the kinetic energy contri-

bution to the Hamiltonian is a 4×4 matrix given by

$$\check{H}_0 = \hat{H}_{RD}(\mathbf{k}_1) \otimes \hat{\mathbb{I}} + \hat{\mathbb{I}} \otimes \hat{H}_{RD}(\mathbf{k}_2), \quad (2)$$

where \mathbf{k}_i with $i \in \{1, 2\}$ is the momentum of the i -th particle and the check indicates an operator acting on the two-particle Hilbert space. For some interaction Hamiltonian \check{H}_{int} the total Hamiltonian of the system is then given by $\check{H} = \check{H}_0 + \check{H}_{\text{int}}$.

The energy eigenstates of our two-particle system are four-component spinors and are labeled by two indices, \mathbf{Q} and n , where $\mathbf{Q} = \mathbf{k}_1 + \mathbf{k}_2$ is the centre-of-mass momentum and n labels both the various bound and scattering states. Any energy eigenstate $|\psi_n(\mathbf{Q})\rangle$ can be written as a superposition of momentum eigenstates as

$$|\psi_n(\mathbf{Q})\rangle = \int \frac{d^2\mathbf{k}}{(2\pi)^2} \chi_n(\mathbf{Q}, \mathbf{k}) |\mathbf{Q}, \mathbf{k}\rangle, \quad (3)$$

where $\mathbf{k} = (\mathbf{k}_1 - \mathbf{k}_2)/2$ is the relative momentum. Note here that $\chi_n(\mathbf{Q}, \mathbf{k})$ are four-component spinors owing to the different possible spin states of the two-particle system. We will be using the triplet-single basis, $|S, s_z\rangle = \{|1, +1\rangle, |1, -1\rangle, |10\rangle, |00\rangle\}$, to express the spinor (see (20)), unless otherwise stated. The stationary Schrödinger equation is then

$$[\check{H} - \check{\mathbb{I}}E_n(\mathbf{Q})] |\psi_n(\mathbf{Q})\rangle = 0, \quad (4)$$

where $E_n(\mathbf{Q})$ is the energy of the (\mathbf{Q}, n) state. Inserting (3) into (4), we obtain

$$[\check{H}_0(\mathbf{Q}, \mathbf{k}) - \check{\mathbb{I}}E_n(\mathbf{Q})] \chi_n(\mathbf{Q}, \mathbf{k}) + \int \frac{d^2\mathbf{k}'}{(2\pi)^2} \langle \mathbf{k} | \check{H}_{\text{int}} | \mathbf{k}' \rangle \chi_n(\mathbf{Q}, \mathbf{k}') = 0. \quad (5)$$

We note that a general isotropic interaction in two dimensions can be written as

$$\langle \mathbf{k} | \check{H}_{\text{int}} | \mathbf{k}' \rangle = \sum_{l=-\infty}^{\infty} \check{V}_l(k, k') e^{il(\phi_{\mathbf{k}} - \phi_{\mathbf{k}'})}, \quad (6)$$

where $\phi_{\mathbf{k}}$ is the angle between \mathbf{k} and the x -axis. We will hereafter assume that the interaction is short-ranged. At low energies and long wavelengths, scattering amplitude is dominated by the contribution of the s -wave scattering as long as the relative momentum \mathbf{k} satisfies $kR_e \ll 1$, where R_e is the characteristic radius of the interaction. Due to the anti-symmetry of the two-particle wave function we must project out the singlet component of the wave function for the s -wave component (i.e. $l = 0$). Dropping higher order harmonic contributions, we may then write the potential as $\langle \mathbf{k} | \check{H}_{\text{int}} | \mathbf{k}' \rangle \rightarrow V_0 \check{\mathcal{P}}^{(s)}$, where $\check{\mathcal{P}}^{(s)} = |00\rangle \langle 00|$ is the singlet projector. We are then led to rewriting (5) as

$$[\check{H}_0(\mathbf{Q}, \mathbf{k}) - \check{\mathbb{I}}E_n(\mathbf{Q})] \chi_n(\mathbf{Q}, \mathbf{k}) + V_0 \int \frac{d^2\mathbf{k}'}{(2\pi)^2} \check{\mathcal{P}}^{(s)} \chi_n(\mathbf{Q}, \mathbf{k}') = 0. \quad (7)$$

Let us now define the inverse Green function as $\check{\mathcal{G}}_n^{-1}(\mathbf{Q}, \mathbf{k}) = \check{H}_0(\mathbf{Q}, \mathbf{k}) - \check{\mathbb{I}}E_n(\mathbf{Q})$ and the function $c_{\mathbf{Q}}^n$ via

$$c_{\mathbf{Q}}^n |00\rangle = \int \frac{d^2\mathbf{k}'}{(2\pi)^2} \check{\mathcal{G}}^{(s)} \chi_n(\mathbf{Q}, \mathbf{k}'). \quad (8)$$

Then we obtain the expression for the spinor,

$$\chi_n(\mathbf{Q}, \mathbf{k}) = -c_{\mathbf{Q}}^n V_0 \check{\mathcal{G}}_n(\mathbf{Q}, \mathbf{k}) |00\rangle. \quad (9)$$

The task now is to invert the inverse two-particle Green function, $\check{\mathcal{G}}_n^{-1}(\mathbf{Q}, \mathbf{k})$. Hereafter, we will refrain from writing the index n explicitly since it enters only to label the eigenenergies. We now introduce the single-particle inverse Green functions for particle i , namely, $\hat{g}^{-1}(\mathbf{k}_i, \mathbf{Q}) = \hat{H}_{RD}(\mathbf{k}_i) - \hat{\mathbb{I}}(E_n(\mathbf{Q})/2) = \hat{\mathbb{I}}y(\mathbf{k}_i, \mathbf{Q}) + \alpha\hat{\sigma} \cdot (\mathbf{b}_i \times \hat{z})$, where $y(\mathbf{k}_i, \mathbf{Q}) = \epsilon_{\mathbf{k}_i} - E_n(\mathbf{Q})/2$ and

$$\mathbf{b}_i = \begin{pmatrix} 1 & \gamma \\ \gamma & 1 \end{pmatrix} \mathbf{k}_i. \quad (10)$$

Here, $\gamma = \beta/\alpha$ measures the relative strength between the Rashba and Dresselhaus couplings. The two-particle inverse Green function is then

$$\check{\mathcal{G}}^{-1}(\mathbf{Q}, \mathbf{k}) = \left[\hat{g}^{-1}(\mathbf{k}_1, \mathbf{Q}) \otimes \hat{\mathbb{I}} + \hat{\mathbb{I}} \otimes \hat{g}^{-1}(\mathbf{k}_2, \mathbf{Q}) \right]. \quad (11)$$

$\hat{g}^{-1}(\mathbf{k}_i, \mathbf{Q})$ can be diagonalized using the unitary matrix

$$\hat{u}_i = \exp \left\{ -i \frac{\pi}{4} (\mathbf{n}_i \cdot \hat{\sigma}) \right\}, \quad (12)$$

where $\mathbf{n}_i = \mathbf{b}_i/b_i$. We then obtain $\hat{u}_i^\dagger \hat{g}^{-1}(\mathbf{k}_i, \mathbf{Q}) \hat{u}_i = \hat{\mathbb{I}}y_n(\mathbf{k}_i, \mathbf{Q}) + \alpha b_i \hat{\sigma}_z$. Therefore, $\check{\mathcal{G}}^{-1}(\mathbf{Q}, \mathbf{k})$ can be inverted using the composite unitary transformation $\check{U} = \hat{u}_1 \otimes \hat{u}_2$ and we obtain

$$\check{\mathcal{G}}(\mathbf{Q}, \mathbf{k}) = \check{U} \check{D}(\mathbf{Q}, \mathbf{k}) \check{U}^\dagger \quad (13)$$

with

$$\check{D}(\mathbf{Q}, \mathbf{k}) = \text{Diag} \{ [D_1(\mathbf{Q}, \mathbf{k})]^{-1}, [D_2(\mathbf{Q}, \mathbf{k})]^{-1}, [D_3(\mathbf{Q}, \mathbf{k})]^{-1}, [D_4(\mathbf{Q}, \mathbf{k})]^{-1} \}, \quad (14)$$

and

$$D_1(\mathbf{Q}, \mathbf{k}) = s + \alpha(b_1 + b_2) \quad (15)$$

$$D_2(\mathbf{Q}, \mathbf{k}) = s + \alpha(b_1 - b_2) \quad (16)$$

$$D_3(\mathbf{Q}, \mathbf{k}) = s - \alpha(b_1 - b_2) \quad (17)$$

$$D_4(\mathbf{Q}, \mathbf{k}) = s - \alpha(b_1 + b_2). \quad (18)$$

Here, we have defined

$$s := s(\mathbf{Q}, \mathbf{k}) = \frac{k^2}{m} + \frac{Q^2}{4m} - E_n(\mathbf{Q}), \quad (19)$$

An explicit expression for the Green function matrix (13) is presented in Appendix A. Inserting (13) into (9) the

spinor $\chi(\mathbf{Q}, \mathbf{k})$ can be expressed in the triplet-singlet basis as

$$\chi(\mathbf{Q}, \mathbf{k}) = -\frac{c_{\mathbf{Q}} V_0}{d(\mathbf{Q}, \mathbf{k})} \begin{pmatrix} \mathcal{A}_1^t(\mathbf{Q}, \mathbf{k}) \\ -\mathcal{A}_1^{t*}(\mathbf{Q}, \mathbf{k}) \\ \mathcal{A}_0^t(\mathbf{Q}, \mathbf{k}) \\ \mathcal{A}^s(\mathbf{Q}, \mathbf{k}) \end{pmatrix}. \quad (20)$$

The denominator $d(\mathbf{Q}, \mathbf{k})$ is given by

$$d(\mathbf{Q}, \mathbf{k}) = s^4 - 4\alpha^2 s^2 \left(b^2 + \frac{B^2}{4} \right) + 4\alpha^4 (\mathbf{B} \cdot \mathbf{b})^2, \quad (21)$$

where $\mathbf{B} = \mathbf{b}_1 + \mathbf{b}_2$, $\mathbf{b} = (\mathbf{b}_1 - \mathbf{b}_2)/2$. The coefficients for the triplet and singlet components are explicitly given by

$$\mathcal{A}_1^t(\mathbf{Q}, \mathbf{k}) = i\sqrt{2} [s\alpha b e^{-i\phi_b} - \alpha^3 (\mathbf{B} \cdot \mathbf{b}) B e^{-i\phi_B}] \quad (22)$$

$$\mathcal{A}_0^t(\mathbf{Q}, \mathbf{k}) = 2is\alpha^2 [\mathbf{B} \times \mathbf{b}]_z \quad (23)$$

$$\mathcal{A}^s(\mathbf{Q}, \mathbf{k}) = s(s^2 - \alpha^2 B^2), \quad (24)$$

where $\phi_b = \tan^{-1}(b_y/b_x)$ and similarly for ϕ_B . Note that both $\mathcal{A}_1^t(\mathbf{Q}, \mathbf{k})$ and $\mathcal{A}_0^t(\mathbf{Q}, \mathbf{k})$ are odd functions of the relative momentum \mathbf{k} , while $\mathcal{A}^s(\mathbf{Q}, \mathbf{k})$ is even. This ensures that the wave function $\chi(\mathbf{Q}, \mathbf{k})$ is anti-symmetric under interchange of two particles: $\mathbf{Q} \rightarrow \mathbf{Q}$, $\mathbf{k} \rightarrow -\mathbf{k}$ and $\sigma_1 \leftrightarrow \sigma_2$. (20) together with the Green function (A1) represent the exact solution, and is the main new technical result of this work.

The normalization constant $c_{\mathbf{Q}}$ can be obtained from the orthonormality condition for the energy eigenstates $|\psi(\mathbf{Q})\rangle$, i.e. $\langle \psi(\mathbf{Q}) | \psi(\mathbf{Q}) \rangle = \langle \mathbf{Q} | \mathbf{Q} \rangle$ for all \mathbf{Q} (and n),

$$|c_{\mathbf{Q}}|^2 = \left[V_0^2 \int \frac{d^2\mathbf{k}}{(2\pi)^2} \langle 00 | \check{\mathcal{G}}^\dagger(\mathbf{Q}, \mathbf{k}) \check{\mathcal{G}}(\mathbf{Q}, \mathbf{k}) | 00 \rangle \right]^{-1}. \quad (25)$$

The solution is complete once the energy spectrum $E_n(\mathbf{Q})$ is obtained for all the eigenstates.

III. PROPERTIES OF THE BOUND MOLECULAR STATE

If an energy eigenstate (\mathbf{Q}, n) describes a bound state of our two fermion system its spectrum must satisfy $E_n(\mathbf{Q}) < 2E_{\min}$ for some values of \mathbf{Q} . Here, E_{\min} is the minimum value in the single-fermion spectrum for Hamiltonian (1), which is

$$E_{\mathbf{k}} = \frac{k^2}{2m} \pm \alpha k \sqrt{1 + \gamma^2 + 2\gamma \sin(2\phi_k)}, \quad (26)$$

where $\phi_k = \tan^{-1}(k_y/k_x)$. We find $E_{\min} = -m\alpha^2(1 + \gamma)^2/2$. $\gamma = \beta/\alpha$, again, is the relative strength between the Rashba and Dresselhaus couplings. We may now define the momentum-dependent binding energy $\Delta_n(\mathbf{Q})$ through $E_n(\mathbf{Q}) = 2E_{\min}(1 + \Delta_n(\mathbf{Q})/m\alpha^2)$. The condition for a bound state then translates to $\Delta_n(\mathbf{Q}) > 0$ for some \mathbf{Q} .

A. The binding energy at $\mathbf{Q} = 0$

Owing to the oddness of the triplet coefficients in (20) with respect to \mathbf{k} , one finds that only the singlet component survives once one integrates over \mathbf{k} in (8). This then leads to the eigenvalue equation for the bound state

$$\int \frac{d^2\mathbf{k}}{(2\pi)^2} \chi(\mathbf{Q}, \mathbf{k}) = c_{\mathbf{Q}} |00\rangle. \quad (27)$$

Making use of (9) leads to the self-consistency condition

$$-\frac{1}{V_0} = \int \frac{d^2\mathbf{k}}{(2\pi)^2} \langle 00 | \mathcal{G}(\mathbf{Q}, \mathbf{k}) | 00 \rangle, \quad (28)$$

which, together with (1), (2) and (A1), has an explicit form

$$\int \frac{d^2\mathbf{k}}{(2\pi)^2} \frac{s(s^2 - \alpha^2 B^2)}{d(\mathbf{Q}, \mathbf{k})} = -\frac{1}{V_0}, \quad (29)$$

Introducing the dimensionless variables,

$$\mathbf{q} = \frac{\mathbf{Q}}{m\alpha}, \quad \boldsymbol{\kappa} = \frac{\mathbf{k}}{m\alpha}, \quad \delta_n = \frac{\Delta_n}{m\alpha^2}, \quad v_0 = mV_0, \quad (30)$$

and the dimensionless energy variable $\xi = \kappa^2$ the self-consistency condition for $\mathbf{q} = 0$ reduces to

$$-\frac{2}{v_0} = \int_0^\lambda \frac{d^2\xi d\phi}{(2\pi)^2} \frac{\xi - e_n(0)}{(\xi - e_n(0))^2 - 4a(\phi)\xi}. \quad (31)$$

Here, we have defined the dimensionless energy spectrum $e_n(\mathbf{q}) = e_t(1 + \delta_n(\mathbf{q}))$, where $e_t = 2e_{\min} = -(1 + \gamma)^2$ is the dimensionless threshold energy and $a(\phi) = 1 + \gamma^2 + 2\gamma \sin 2\phi$. We have also introduced the UV cutoff $\lambda \sim 1/(m\alpha R_e)^2$ which is set by the characteristic radius of the interaction potential R_e . The typical $\delta_n(0)$ -dependence of the right hand side of (31) is plotted in Fig. 1 for $\gamma = 0$, $\gamma = 0.1$ and $\gamma = 0.5$. We find that for any given attractive interaction $v_0 < 0$, there is a *single* bound state. We label this state by $n = 0$, but refrain from explicitly writing the index. For the isotropic case (i.e. $\gamma = 0$) and for $0 < \delta(0) \ll 1$, we find that the binding energy is given by

$$\delta(0) \approx \frac{|v_0|^2}{16} =: \delta^R(0). \quad (32)$$

In the weakly anisotropic regime (i.e. $0 < \gamma/\delta(0) \ll 1$) we find the lowest γ -corrections to be

$$\delta(0) \approx \delta^R(0) \left[1 - 2\frac{\gamma}{\delta^R(0)} + \frac{3}{2} \left(\frac{\gamma}{\delta^R(0)} \right)^2 \right], \quad (33)$$

while in the strongly anisotropic regime (i.e. $\gamma/\delta(0) \gg 1$) we obtain

$$\delta(0) \approx \frac{\lambda}{(1 + \gamma)^2} e^{-\frac{8\pi\sqrt{\gamma}}{|v_0|(1+\gamma)}}. \quad (34)$$

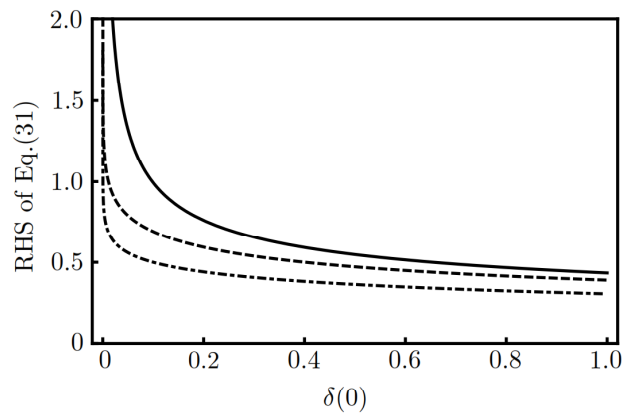


FIG. 1: Plot of the right hand side of (31) as a function of the binding energy $\delta(0) > 0$. Here, we have chosen $\gamma = 0$ for the solid line, $\gamma = 0.1$ for the dashed line and $\gamma = 0.5$ for the dot-dashed line. While an algebraic divergence is observed as $\delta(0) \rightarrow 0$ in the $\gamma = 0$ case, a logarithmic divergence is observed in the presence of the Dresselhaus coupling ($\gamma > 0$). The UV cutoff is $\lambda = 100$.

Here, we have assumed $\lambda \gg 1 + \gamma$. We remind the reader that $\gamma = \beta/\alpha$ is the relative strength between the Rashba and Dresselhaus couplings. Similar calculations for the binding energy have been done previously for various SO coupled Fermi gases.⁴²⁻⁴⁶ However, the consideration of arbitrary two-dimensional Rashba and Dresselhaus coupling strengths in two spatial dimensions and the presentation of the exact wave function, to the best of our knowledge, has not been done.

The crossover in the binding energy from an algebraic dependence on the interaction strength (c.f. (32)) to exponential (c.f. (34)) is directly related to the crossover in *effective dimensionality* for bound state formation.³⁹ Let us say that a SO coupled system in D spatial dimensions has a set of single-particle minimum-energy states in momentum space that forms a d -dimensional surface. The effective dimensionality for bound state formation is given by $D_{\text{eff}} = D - d$. As can be seen from the single-particle spectrum (26) the isotropic case possesses a 1D manifold of minimum states ($d = 1$) while once the Dresselhaus coupling is finite, this manifold of minimum states is reduced to two points in momentum space ($d = 0$). The effective dimensionalities for the two cases are then $D_{\text{eff}} = 1$ and $D_{\text{eff}} = 2$, respectively. The exponentially small binding energy (34) and the effective dimension $D_{\text{eff}} = 2$ corresponding to that case is consistent with a bound state problem in quantum mechanics of a particle moving in a potential well in two dimensions.

The binding energy can also be computed in the regime where $\delta(0) \gg 1$. Since $\gamma \sim 1$, we will simply consider $\gamma = 0$. If the cutoff scale is still the largest scale, such that $\delta(0) \ll \lambda$, we find the binding energy to be

$$\delta(0) \approx \lambda e^{-\frac{4\pi}{|v_0|}}. \quad (35)$$

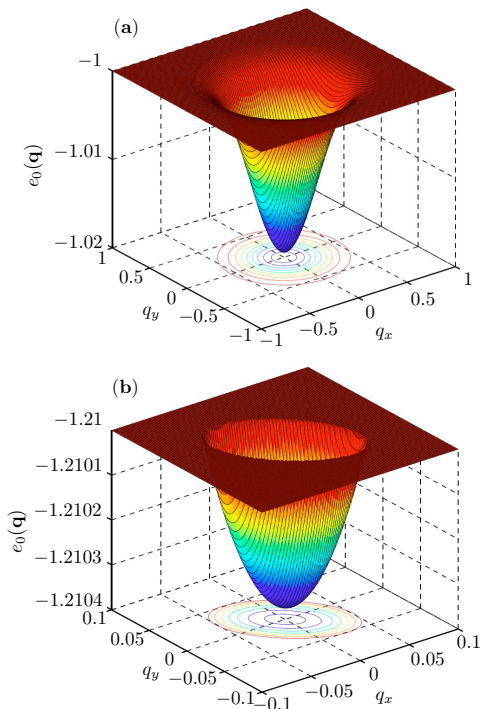


FIG. 2: Numerical results for the dimensionless molecular spectrum $e(\mathbf{q}) = E(\mathbf{Q})/m\alpha^2$ as a function of the dimensionless molecular momentum \mathbf{q} . (a) $\gamma = 0$ and $|v_0|^{-1} = 2$ are used. (b) $\gamma = 0.1$ and $|v_0|^{-1} = 1.5$ are used. Anisotropy in the molecular effective mass can be observed in (b) for finite Dresselhaus coupling (c.f. (38)). The plot shows the bound state ceases to exist for momenta larger than the critical momentum $q_c \sim \sqrt{\delta(0)}$.

B. The molecular spectrum

We first provide an approximate analytic expression for the spectrum valid for $q^2/\delta(0) \ll 1$, from which the effective mass of the molecule can be extracted. In the weakly isotropic limit, the binding energy to $\mathcal{O}(q^2)$ reads

$$\delta(\mathbf{q}) \approx \delta(0) - \frac{q^2}{8} \left[1 + \frac{3}{2} \frac{\gamma}{\delta R(0)} \sin(2\phi_q) \right], \quad (36)$$

where $\phi_q = \tan^{-1}(q_y/q_x)$. For $\gamma = 0$, the isotropy in the spectrum is restored as expected. The corresponding effective mass for the molecule is then given by

$$M_{\text{eff}}(\gamma) \approx 4m \left[1 - \frac{3}{2} \frac{\gamma}{\delta R(0)} \sin(2\phi_q) \right]. \quad (37)$$

In the strongly anisotropic regime, the binding energy to $\mathcal{O}(q^2)$ reads

$$\delta(\mathbf{q}) \approx \delta(0) - \frac{q^2}{8} \frac{1 + 6\gamma + \gamma^2 + (1 - \gamma)^2 \sin(2\phi_q)}{(1 + \gamma)^4}, \quad (38)$$

with the corresponding effective mass of

$$M_{\text{eff}}(\gamma) \approx \frac{4m(1 + \gamma)^2}{1 + 6\gamma + \gamma^2 + (1 - \gamma)^2 \sin(2\phi_q)}. \quad (39)$$

Interestingly, we find that isotropy in the effective mass is restored for equal Rashba and Dresselhaus interaction strengths ($\gamma = 1$), the so-called persistent spin helix point^{55–57}. Let us now consider the effective mass of a free fermion, $m_{\text{eff}}(\gamma)$, near the bottom of the single-particle spectrum (26). We find that the *molecular* effective mass and the *single-fermion* effective mass are related in a one-to-one relation, namely, $M_{\text{eff}}(\gamma) = 2m_{\text{eff}}(\gamma)$. The dimensionless molecular spectrum $e(\mathbf{q}) = E(\mathbf{Q})/m\alpha^2$ can be straightforwardly obtained through the relation $e(\mathbf{q}) = e_t(1 + \delta(\mathbf{q}))$.

The molecular spectrum can be obtained numerically for arbitrary values of \mathbf{q} . The results for the spectrum as a function of \mathbf{q} are plotted in Fig. 2 for $\gamma = 0$ and $\gamma = 0.1$, respectively. $|v_0|$ was chosen to be $\mathcal{O}(1)$ such that we are in the regime of $\delta(0) \ll 1$. We see the anisotropy in the spectrum for $\gamma = 0.1$ (Fig. 2(b)). We also see that for large enough momenta, $q > q_c$, a bound state ceases to exist. The scale for the critical momentum is set by $q_c \sim \sqrt{\delta(0)}$. The existence of this critical momentum tells us that the fermions do not remain bound once the molecular kinetic energy exceeds the binding energy.

An estimate of the binding energy can be made if a gas of these fermionic molecules is rotated. We consider the gas confined to the xy -plane and a rotation about the z -axis. For simplicity, we will take the pure Rashba case here, i.e. $\gamma = 0$. In the dilute limit, where the gas can be treated as a classical (Maxwell-Boltzmann) gas, the velocity field under the rotation $\mathbf{\Omega} = \Omega \mathbf{z}$ is given by a rigid rotation $\mathbf{v}(R) = \Omega R \phi$, where ϕ is the unit tangent vector on the xy -plane and $R = \sqrt{x^2 + y^2}$ is the radial distance from the axis of rotation. The critical momentum scale then introduces a critical distance scale R_c , where, for $R < R_c$, the molecules are still bound but, for $R > R_c$, we have a gas of unbound fermions. If we introduce a dimensionless distance $r = R\Omega/\alpha$ the critical distance is given by $r_c = q_c/4 \sim \sqrt{\delta(0)}$. Therefore, the radial distance at which the two phases of bound and unbound fermions meet gives an estimate of the binding energy.

C. Effects due to a Zeeman field

We briefly discuss the effects of a synthetic Zeeman field, $\mathbf{H} = (H_x, H_y, H_z)$, which couples to the pseudo-spin of the fermions. We introduce a Zeeman term, $\hat{H}_Z = -(H_x \hat{\sigma}_x + H_y \hat{\sigma}_y + H_z \hat{\sigma}_z)$ to the single-particle Hamiltonian (1). In Appendix B the self-consistency condition is rederived for a Zeeman field oriented in a general direction in \mathbb{R}^3 . Here, we will explicitly consider the field pointing in the z -direction, and for the pure Rashba case where $\gamma = 0$. We find that the self-consistency condition

at $\mathbf{q} = 0$ is given by

$$-\frac{2}{v_0} = \int_0^\lambda \frac{d^2\xi}{2\pi} \frac{(\xi - e_0(0))^2 - 4h^2}{(\xi - e_0(0))[(\xi - e_0(0))^2 - 4\xi - 4h^2]}, \quad (40)$$

where the dimensionless Zeeman field $h = H/m\alpha^2$. Since the threshold energy for molecular formation is now $e_t = -(1+h^2)$, the dimensionless energy for the bound state at $\mathbf{q} = 0$ reads $e_0(0) = -(1+h^2)(1+\delta(0))$. For $h < h_c = 1$, (40) gives

$$-\frac{4}{v_0} \approx \frac{1-h^2}{\sqrt{1+h^2}} \frac{1}{\sqrt{\delta(0)}}, \quad (41)$$

where again the approximation holds for $\delta(0) \ll 1$ and $\lambda \gg 1$. For $h < h_c$, a bound state exists for all $|v_0|$, but the binding energy approaches zero as $h \rightarrow h_c$. Once $h > h_c$, the integral on the right hand side of (40) becomes bounded as $\delta(0) \rightarrow 0$ and, therefore, a bound state ceases to exist for sufficiently weak attractive interaction strengths. This introduces a quantum phase transition at a critical coupling v_0^c separating phases with bound and unbound fermions.

IV. LOW-DENSITY RASHBA-DRESELHAUS MOLECULAR GAS

Let us now consider a low-density gas of N tightly-bound Rashba-Dresselhaus molecules confined to two spatial dimensions. We assume that the gas is equilibrated at some temperature T , which satisfies $T_{BKT} \ll T \ll \Delta$. Here, T_{BKT} is the temperature at which the gas undergoes a Berezinskii-Kosterlitz-Thouless phase transition into a superfluid, and Δ is the molecular binding energy. Presumably, in this temperature range, the gas is in the dilute limit, $n\lambda_T^2 \ll 1$, where n is the areal density of the molecules and $\lambda_T = h/\sqrt{2\pi\mathcal{M}k_B T}$, with $\mathcal{M} := \min\{M_{\text{eff}}(\gamma)\}$, is the mean thermal wavelength evaluated for the smallest molecular effective mass. The gas may then be modeled as a thermal Boltzmann gas of uncondensed molecules.

A molecule can interact with other atoms and molecules in the gas. Indeed, scattering between atoms and bound molecules as well as between two molecules was considered in depth in many works.^{58–62} Here, we assume that the gas is sufficiently dilute so that we may neglect atom-molecule and molecule-molecule interactions to first order.

Our aim first is to obtain TOF velocity and spin distributions for a single fermion atom for the molecular gas. These distributions can be inferred from a spin-resolved TOF experiment, where both the trap and the SO coupling are turned off and the *depaiored* fermions are allowed to expand freely. We then contrast these distributions to corresponding distributions for a Boltzmann gas of unbound (non-interacting) fermionic atoms and discuss the striking differences between the two cases.

A. Qualitative discussion of the result

For the gas of non-interacting molecules (“gas A ”) single-fermion distributions must be extracted from the *single-molecule* density matrix. For the gas of non-interacting fermion atoms (“gas B ”) the corresponding distributions are obtained directly from the *single-fermion* density matrix. For gas A the single-molecule density matrix is given by

$$\hat{\rho}_A = \frac{e^{-\beta\check{H}}}{\text{Tr}\{e^{-\beta\check{H}}\}}, \quad (42)$$

where the Hamiltonian $\check{H} = \check{H}_0 + \check{H}_{\text{int}}$ was given in (2) and (6) in Sec. II. For gas B , the single-fermion density matrix reads

$$\hat{\rho}_B = \frac{e^{-\beta\check{H}_{RD}}}{\text{Tr}\{e^{-\beta\check{H}_{RD}}\}}, \quad (43)$$

where the Hamiltonian was given in (1). The key difference in the single-fermion distributions for gases A and B stems from the fact that while the single-fermion momentum eigenstate for gas B , $|\mathbf{k}\rangle$, is an eigenstate of \check{H}_{RD} , the two-fermion momentum eigenstate, $|\mathbf{Q}, \mathbf{k}\rangle$, for gas A is not an eigenstate of \check{H} . For gas B the momentum operator commutes with the Hamiltonian, and the velocity distribution for the Boltzmann gas is trivially given by

$$P(\mathbf{k}) = \langle \mathbf{k} | \hat{\rho}_B | \mathbf{k} \rangle \propto e^{-\beta E_{\mathbf{k}}}, \quad (44)$$

where $E_{\mathbf{k}}$ was given in (26). For gas A , we first obtain the diagonal elements of the molecular density matrix, $\langle \mathbf{Q}, \mathbf{k} | \hat{\rho}_A | \mathbf{Q}, \mathbf{k} \rangle$, and the velocity distribution is extracted by tracing out one of the fermions. Since $|\mathbf{Q}, \mathbf{k}\rangle$ is not an eigenstate of \check{H} , we must introduce the energy eigenstates $|\psi_n(\mathbf{Q})\rangle$ in order to replace \check{H} by its expectation value. This results in the diagonal elements which schematically has the form

$$P(\mathbf{k}_1, \mathbf{k}_2) = \langle \mathbf{Q}, \mathbf{k} | \hat{\rho}_A | \mathbf{Q}, \mathbf{k} \rangle \propto \chi^\dagger(\mathbf{Q}, \mathbf{k}) \chi(\mathbf{Q}, \mathbf{k}) e^{-\beta E(\mathbf{Q})}, \quad (45)$$

where $E(\mathbf{Q})$ is the molecular spectrum obtained in Sec. IIIB and $\chi(\mathbf{Q}, \mathbf{k})$ is the spinor wave function obtained in (20). The extra factor involving χ in (45) indicates that each fermion is correlated with its partner fermion due to interactions. In the free fermion case (c.f. (44)), such correlations are clearly absent.

The correlations between fermions in gas A has an imprint on the various momentum distributions and make them distinct from the corresponding distributions in gas B . Moreover, these distinctions can be made within first-moment expectation values (e.g. $\langle n(\mathbf{k}) \rangle$). These differences can, in principle, be inferred from TOF experiments. For small binding energies (i.e. $\delta(0) \ll 1$) the *qualitative* shapes of the various momentum distributions, in general, appear similar for both gases. The key

difference arises in the width of the peak features found in the distributions. For free fermions (gas B) these peak features should have a gaussian profile with the width set by temperature, as it is clear from (44). In contrast, the peak features for gas A has a square-Lorentzian profile with the width set by the binding energy scale. In fact, for gas A , the peak features are determined by the wave function $\chi(\mathbf{Q}, \mathbf{k})$, and not the Boltzmann factor, which primarily determines the centre-of-mass distribution of the molecules (c.f. (45)).

For $\tau := k_B T / m \alpha^2 \ll \delta(0)$, the width in the peak structures for gas A should be markedly broader than those for gas B . The peak widths for gas B can be adjusted by changing the temperature while such variation should not occur for gas A . On the other hand, increasing the attractive interaction strength, thus increasing the binding energy, while holding the temperature fixed should lead to a broadening in the width of the peaks for gas A only.

B. Quantitative results for various distributions

We now provide detailed calculations of the single-fermion distributions for gas A described above. Recall that the (dimensionless) molecular dispersion was given by $e(\mathbf{q}) = e_t(1 + \delta(\mathbf{q}))$, with \mathbf{q} -dependent binding energies (36) or (38) which are valid for $q^2 \ll \delta(0)$. The validity of (36) or (38) is ensured in our temperature regime, since $\tau = k_B T / m \alpha^2 \ll \delta(0)$, such that essentially all of the fermions are bound and occupy single-molecule states very close to $\mathbf{q} = 0$. The diagonal elements of the single-molecule density matrix (42) can then be approximately written as (see Appendix C)

$$P(\boldsymbol{\kappa}_1, \boldsymbol{\kappa}_2) \approx \frac{|c_{\mathbf{q}}|^2 \langle 00 | \mathcal{G}^\dagger(\mathbf{q}, \boldsymbol{\kappa}) \mathcal{G}(\mathbf{q}, \boldsymbol{\kappa}) | 00 \rangle e^{-e(\mathbf{q})/\tau}}{\int_{\mathbf{q}, \boldsymbol{\kappa}} |c_{\mathbf{q}}|^2 \langle 00 | \mathcal{G}^\dagger(\mathbf{q}, \boldsymbol{\kappa}) \mathcal{G}(\mathbf{q}, \boldsymbol{\kappa}) | 00 \rangle e^{-e(\mathbf{q})/\tau}}, \quad (46)$$

where $\int_{\mathbf{q}, \boldsymbol{\kappa}} = \int \frac{d^2 \mathbf{q}}{(2\pi)^2} \frac{d^2 \boldsymbol{\kappa}}{(2\pi)^2}$. Here again, \mathbf{q} and $\boldsymbol{\kappa}$ are dimensionless momenta and $\mathbf{q} = \boldsymbol{\kappa}_1 + \boldsymbol{\kappa}_2$ and $\boldsymbol{\kappa} = (\boldsymbol{\kappa}_1 - \boldsymbol{\kappa}_2)/2$. The velocity distribution for a single fermion can be obtained by integrating out the other,

$$P(\boldsymbol{\kappa}_1) = \int \frac{d^2 \boldsymbol{\kappa}_2}{(2\pi)^2} P(\boldsymbol{\kappa}_1, \boldsymbol{\kappa}_2). \quad (47)$$

Note that $P(\boldsymbol{\kappa}_1, \boldsymbol{\kappa}_2) = P(\boldsymbol{\kappa}_2, \boldsymbol{\kappa}_1)$ so one could have integrated out either one or the other electron and would have arrived at the same probability.

The single-fermion spin distributions can also be obtained analogously. The three spin operators for a fermion are $\hat{S}_i = \hat{\sigma}_i/2$, where $i = x, y, z$. The i -th com-

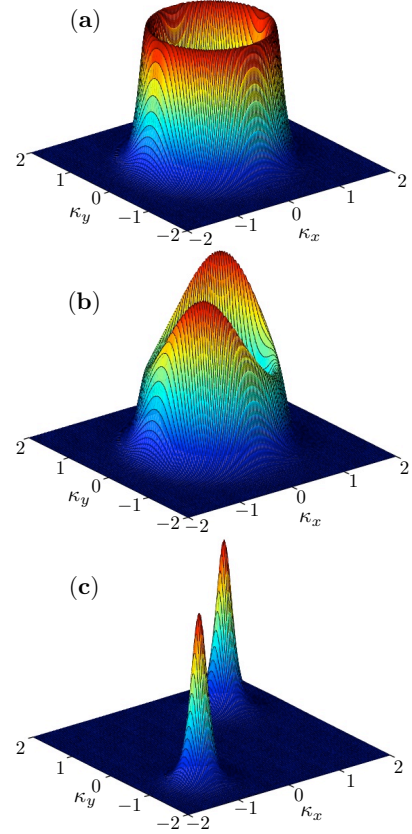


FIG. 3: Single-fermion velocity distribution for the molecular gas for three different relative SO interaction strengths: (a) $\gamma = 0$; (b) $\gamma = 0.005$; and (c) $\gamma = 0.5$. Binding energy $\delta(0) = 0.05$ is used, and the temperature is taken to be small such that $\tau \ll \delta(0)$.

ponent of the spin density is then given by

$$S_i(\boldsymbol{\kappa}_1) := \langle \hat{S}_i \rangle(\boldsymbol{\kappa}_1) = \int \frac{d^2 \boldsymbol{\kappa}_2}{(2\pi)^2} \times \frac{|c_{\mathbf{q}}|^2 \langle 00 | \mathcal{G}^\dagger(\mathbf{q}, \boldsymbol{\kappa}) [\hat{S}_i \otimes \hat{\mathbb{I}}] \mathcal{G}(\mathbf{q}, \boldsymbol{\kappa}) | 00 \rangle e^{-e(\mathbf{q})/\tau}}{\int_{\mathbf{q}, \boldsymbol{\kappa}} |c_{\mathbf{q}}|^2 \langle 00 | \mathcal{G}^\dagger(\mathbf{q}, \boldsymbol{\kappa}) \mathcal{G}(\mathbf{q}, \boldsymbol{\kappa}) | 00 \rangle e^{-e(\mathbf{q})/\tau}}, \quad (48)$$

Note here that the matrix $\hat{S}_i \otimes \hat{\mathbb{I}}$ acts in spin space spanned by the basis $|\sigma_1, \sigma_2\rangle = \{|\uparrow\uparrow\rangle, |\uparrow\downarrow\rangle, |\downarrow\uparrow\rangle, |\downarrow\downarrow\rangle\}$. We find that $S_z(\boldsymbol{\kappa}_1) = 0$, which is expected from solving a single-fermion quantum mechanical problem with Hamiltonian (1).

At low temperatures but still well above T_{BKT} , the Boltzmann factor in (47) and (48) is a strongly peaked function at $\mathbf{q} = 0$ with contributions becoming exponentially small for $q > \sqrt{\tau}$. In the low temperature regime we are considering ($\tau \ll \delta(0)$) the remaining factors in (47) and (48) give a slowly-varying function of \mathbf{q} on the scale of $\sqrt{\tau}$. We may then drop the \mathbf{q} -dependence in those factors and replace it by 0. As a result, the integral over $\boldsymbol{\kappa}_2$ can be done trivially and we arrive at

$$P(\boldsymbol{\kappa}) \approx C \langle 00 | \mathcal{G}^\dagger(0, \boldsymbol{\kappa}) \mathcal{G}(0, \boldsymbol{\kappa}) | 00 \rangle, \quad (49)$$

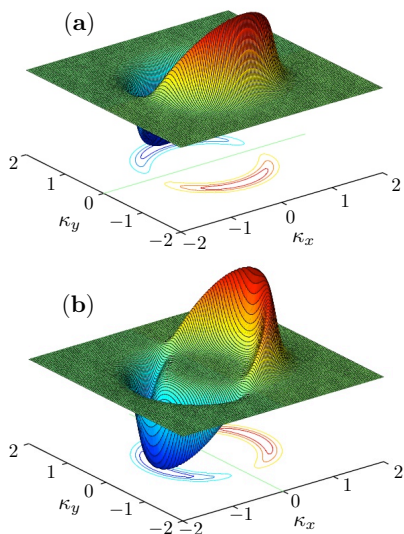


FIG. 4: Single-fermion spin densities in momentum space for $\gamma = 0$. $S_x(\boldsymbol{\kappa})$ and $S_y(\boldsymbol{\kappa})$ are plotted in (a) and (b), respectively. Binding energy $\delta(0) = 0.05$ is used, and the temperature is taken to be small such that $\tau \ll \delta(0)$.

where C is a normalization constant. Similarly, the spin densities can be approximately written as

$$S_i(\boldsymbol{\kappa}) \approx C \langle 00 | \mathcal{G}^\dagger(0, \boldsymbol{\kappa}) [\hat{S}_i \otimes \mathbb{I}] \mathcal{G}(0, \boldsymbol{\kappa}) | 00 \rangle. \quad (50)$$

C. Velocity distribution

Plots of $P(\boldsymbol{\kappa})$ are shown in Fig. 3 for three different values of γ : (a) $\gamma = 0$; (b) $\gamma = 0.005$; and (c) $\gamma = 0.5$. The $\mathbf{q} = 0$ binding energy was taken to be $\delta(0) = 0.05$ and $\tau = 10^{-6}$. We find that the maxima in the velocity distributions occur for values of momenta where the minima in the single-particle spectrum (26) occur. For $\gamma = 0$ the spectrum has a ring of degenerate minima at $\kappa = 1$, and this is reflected in the distribution in Fig. 3(a). The Dresselhaus interaction breaks this degeneracy and the spectrum yields two minima at $(\kappa_x, \kappa_y) = \pm(1 + \gamma, 1 + \gamma)/\sqrt{2}$. The two peaks in Fig. 3(c) coincide again with the locations of these minima. The distribution in the crossover regime between the isotropic and strongly anisotropic limits is plotted in Fig. 3(b).

The fact that large weights are observed at spectrum minima is expected as we are in the dilute and low temperature limits where most of the fermions are occupying momentum states near the band minima. Although corresponding distributions for free fermions (gas B) will be qualitatively similar to the distributions obtained here for gas A , they are quantitatively different. For the pure Rashba case ($\gamma = 0$), for instance, the width of the ring of maxima for gas B is set by the temperature (c.f. (44)).

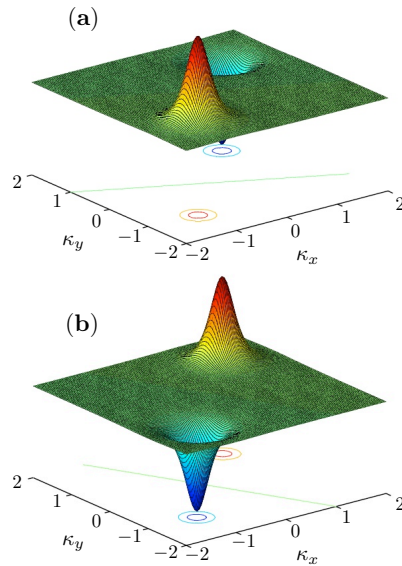


FIG. 5: Single-fermion spin densities in momentum space for $\gamma = 0.5$. $S_x(\boldsymbol{\kappa})$ and $S_y(\boldsymbol{\kappa})$ are plotted in (a) and (b), respectively. Binding energy $\delta(0) = 0.05$ is used, and the temperature is taken to be small such that $\tau \ll \delta(0)$.

In particular, the peak profile has a gaussian profile with the width set by $\sqrt{\tau}$. In contrast, for gas A , a radial cut of the velocity distribution is essentially proportional to $\chi^\dagger(0, \boldsymbol{\kappa})\chi(0, \boldsymbol{\kappa})$ and yields

$$\begin{aligned} P(\kappa) &\propto \frac{(\kappa^2 + 1 + \delta(0))^2 + 4\kappa^2}{[(\kappa + 1)^2 + \delta(0)]^2 [(\kappa - 1)^2 + \delta(0)]^2} \\ &\approx \frac{(2 + \delta(0))^2 + 4}{[4 + \delta(0)]^2 [(\kappa - 1)^2 + \delta(0)]^2} \end{aligned} \quad (51)$$

for $\delta(0) \ll 1$. Therefore, the ring of maxima has a square-Lorentzian profile with the width set by $\sqrt{\delta(0)}$. In the limit $\delta(0) \gg \tau$, we would thus expect the peak width to be much broader for gas A than the corresponding distribution for gas B . If $\delta(0)$ is gradually increased while keeping the temperature fixed the ring of maxima for the molecular gas will get progressively broader. Once $\delta(0) \gg 1$, the ring can no longer be resolved and one obtains a single broad peak centred at $\boldsymbol{\kappa} = 0$. This is illustrated in Fig. 6(a) where we have evaluated (49) for $\delta(0) = 5$ (c.f. (35)). This evolution of the velocity distribution as $\delta(0)$ is increased is unique to that molecular gas, for, in the case of free fermions, the ring of maxima should remain sharp with the width set by $\sqrt{\tau}$.

D. Spin density distributions

Spin densities in momentum space, $S_x(\boldsymbol{\kappa})$ and $S_y(\boldsymbol{\kappa})$, are plotted in Figs. 4 and 5 for the regime $\tau \ll \delta(0) \ll 1$. We consider $\gamma = 0$ and $\gamma = 0.5$ in Figs. 4 and 5, respectively. In analogy to the velocity distribution, the

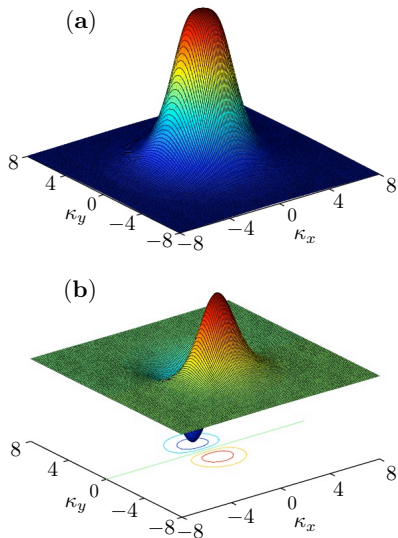


FIG. 6: Single-fermion velocity and S_x distributions with $\gamma = 0$ in the large binding energy limit (i.e. $\delta(0) \gg 1$); here, we have taken $\delta(0) = 5$, and the temperature is still taken to be small such that $\tau \ll 1$.

spin-densities obtained here appear very similar to the corresponding spin-densities obtained by solving a single-fermion quantum mechanical problem with Hamiltonian (1). However, again as in the case of the velocity distribution, the widths of the maxima are set by the binding energy scale. In Fig. 6(b), S_x density for the pure Rashba case is plotted for $\delta(0) = 5$. There, the half-rings of maxima and minima, as seen in Fig. 4(a), are no longer resolved due to the large binding energy.

E. Detecting the distributions in TOF experiments

These momentum distributions will be directly observable through a spin-resolved TOF measurement.³² The TOF signature will be dependent on the SO scheme used. In what follows we assume the effective SO coupling is induced using the N -level scheme, with $N = 4^{63}$, which can be implemented in the alkalis such as ^6Li . In this scheme, the dressed states have the form

$$|D_a\rangle = \frac{1}{2} \sum_{j=1}^4 e^{i\pi a j/2} |\tilde{j}\rangle \quad (52)$$

where $|\tilde{j}\rangle = e^{i\mathbf{K}_j \cdot \mathbf{r}} |j\rangle$ is a bare hyperfine state, $|j\rangle$, boosted by $\mathbf{K}_j = m\alpha[-\sin(\pi j/2)\mathbf{e}_x + \cos(\pi j/2)\mathbf{e}_y]$. The two pseudo-spin states are given by $|\uparrow\rangle = |D_1\rangle$ and $|\downarrow\rangle = |D_2\rangle$.

The velocity-spin distributions shown in Fig. 4 and 5 can be inferred through a spin-resolved TOF measurement. Such a measurement will give the velocity distribution $\langle |j\rangle \langle j| \rangle = \langle \frac{1}{4} \sum_{a=1}^4 e^{-i\pi(a-a')j/2} |D_a\rangle \langle D_{a'}| \rangle$. At

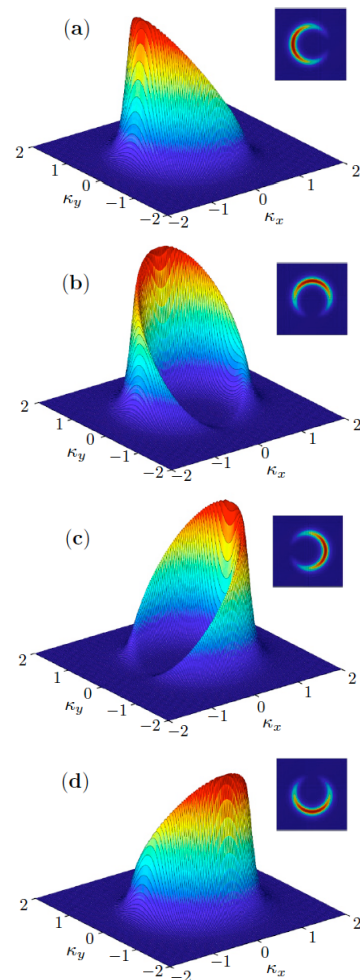


FIG. 7: Single-fermion velocity distribution for the four bare spin states $|1\rangle, |2\rangle, |3\rangle, |4\rangle$ are plotted in (a), (b), (c) and (d), respectively, for $\gamma = 0$ in the small binding energy regime (i.e. $\delta(0) \ll 1$). Here, $\delta(0) = 0.05$ is used, and the temperature is taken to be small such that $\tau \ll \delta(0)$.

low temperatures the state $|D_3\rangle$ and $|D_4\rangle$ will not be populated, and the expectation value reduces to $\langle |j\rangle \langle j| \rangle = \frac{1}{4} \langle |\uparrow\rangle \langle \uparrow| + |\downarrow\rangle \langle \downarrow| + e^{i\pi j/2} |\uparrow\rangle \langle \downarrow| + e^{-i\pi j/2} |\downarrow\rangle \langle \uparrow| \rangle$. These states have the equivalent momentum distributions

$$\langle \mathcal{P}_1 \rangle(\boldsymbol{\kappa}) = \frac{1}{4} (P(\boldsymbol{\kappa}) - 2S_y(\boldsymbol{\kappa})) \quad (53)$$

$$\langle \mathcal{P}_2 \rangle(\boldsymbol{\kappa}) = \frac{1}{4} (P(\boldsymbol{\kappa}) - 2S_x(\boldsymbol{\kappa})) \quad (54)$$

$$\langle \mathcal{P}_3 \rangle(\boldsymbol{\kappa}) = \frac{1}{4} (P(\boldsymbol{\kappa}) + 2S_y(\boldsymbol{\kappa})) \quad (55)$$

$$\langle \mathcal{P}_4 \rangle(\boldsymbol{\kappa}) = \frac{1}{4} (P(\boldsymbol{\kappa}) + 2S_x(\boldsymbol{\kappa})) \quad (56)$$

where $\mathcal{P}_j = |j\rangle \langle j|$ is a projective measurement into the bare spin state $|j\rangle$. It is therefore possible to reconstruct the $P(\boldsymbol{\kappa})$, $S_x(\boldsymbol{\kappa})$ and $S_y(\boldsymbol{\kappa})$ momentum distributions from a TOF measurement.

These spin distributions are plotted in Figs. 7 and 8.

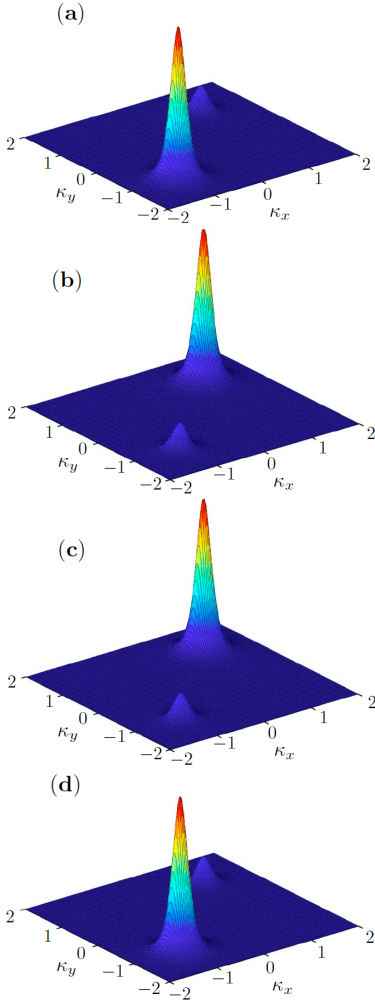


FIG. 8: Single-fermion velocity distribution for the four bare spin states $|1\rangle, |2\rangle, |3\rangle, |4\rangle$ are plotted in (a), (b), (c) and (d), respectively, for $\gamma = 0.5$ in the small binding energy regime (i.e. $\delta(0) \ll 1$). Here, $\delta(0) = 0.05$ is used, and the temperature is taken to be small such that $\tau \ll \delta(0)$.

In the pure Rashba limit, the momentum distribution of the four bare states have the same structure up to a $\pi/2$ rotation in momentum space. In the anisotropic limit, $\gamma \neq 0$, the bare spins have the same two-peak structure, but with different relative amplitudes. Similar to

the momentum distribution, the bare spin distribution can be distinguished from the case of non-interacting SO coupled fermions by the dependence of the width of the distribution on the interaction strength.

V. CONCLUSION

We investigate the properties of a low-density molecular gas of Rashba-Dresselhaus fermions in two spatial dimensions. The gas is considered at sufficiently high temperatures such that it can be considered as a thermal gas of uncondensed tightly bound molecules. The description of the gas is based on the exact solution to a quantum mechanical problem of two Rashba-Dresselhaus fermions interacting via an attractive short-ranged s -wave interaction. We compute the single-fermion density matrix for the gas and evaluate the fermion velocity and spin distributions. By making comparisons to corresponding distributions for a Boltzmann gas of free fermions we show that these various distributions can be used to probe pairing of fermions in the molecular gas. Moreover, we find that the signatures of pairing appear in first-moment expectation values. We discuss a spin-resolved TOF measurement from which the various distributions can be inferred in an experiment. This result is not specific to SO coupled systems considered in this work. Analogous signatures of correlations should appear generally in single-fermion distributions for a system composed of interacting fermions.

Acknowledgments: V. G. would like to thank P. Bedaque for discussions. This research was supported by U.S.-ARO (S. T. & V. G.), ARO-JQI-MURI (B. M. A. & C.-H. L.), ARO-DARPA-OLE (C.-H. L.) and NSF-JQI-PFC (C.-H. L.).

Appendix A: Explicit expression for the Green function matrix (13)

Recall that the Green function matrix was given by $\check{\mathcal{G}}(\mathbf{Q}, \mathbf{k}) = \check{U}\check{D}(\mathbf{Q}, \mathbf{k})\check{U}^\dagger$, where $\check{U} = \hat{u}_1 \otimes \hat{u}_2$, and \hat{u}_i and $\check{D}(\mathbf{Q}, \mathbf{k})$ were defined in (12) and (14), respectively. We then find

$$\check{\mathcal{G}}(\mathbf{Q}, \mathbf{k}) = \frac{1}{4} \begin{pmatrix} (+ + + +) & ie^{-i\phi_2}(+ - + -) & ie^{-i\phi_1}(+ + - -) & -e^{-i(\phi_1+\phi_2)}(+ - - +) \\ -ie^{i\phi_2}(+ - + -) & (+ + + +) & e^{i(\phi_2-\phi_1)}(+ - - +) & ie^{-i\phi_1}(+ + - -) \\ -ie^{i\phi_1}(+ + - -) & e^{i(\phi_1-\phi_2)}(+ - - +) & (+ + + +) & ie^{-i\phi_2}(+ - + -) \\ -e^{i(\phi_1+\phi_2)}(+ - - +) & -ie^{i\phi_1}(+ + - -) & -ie^{i\phi_2}(+ - + -) & (+ + + +) \end{pmatrix}, \quad (\text{A1})$$

where $\phi_i = \tan^{-1}(b_{y,i}/b_{x,i})$, and

$$(p_1 p_2 p_3 p_4) = \sum_{i=1}^4 p_i D_i. \quad (\text{A2})$$

Here, $p_i = \pm 1$ and D_i were defined in (15)-(18).

Appendix B: Self-consistency condition with a Zeeman field

In this appendix, we give a brief derivation of the self-consistency condition in the presence of a Zeeman term of the form $H_Z = -\mathbf{H} \cdot \hat{\boldsymbol{\sigma}}$, where $\hat{\boldsymbol{\sigma}} = (\hat{\sigma}_x, \hat{\sigma}_z)$. The inverse single-particle Green function in this case can be written as $\hat{g}^{-1}(\mathbf{k}_i, \mathbf{Q}) = \hat{1}y(\mathbf{k}_i, \mathbf{Q}) + \alpha \hat{\boldsymbol{\sigma}} \cdot (\bar{\mathbf{b}}_i \times \hat{z}) - H_z \hat{\sigma}_z$, where

$$\bar{\mathbf{b}}_i = \mathbf{b}_i + \frac{1}{\alpha} \mathbf{H}' =: (\mathbf{b}'_i, b_{z,i}), \quad (\text{B1})$$

where $\mathbf{H}' = (-H_x, -H_y, H_z)$. It can be diagonalized with a unitary transformation

$$\hat{u}_i = \exp \left\{ -\frac{i}{4} \left[\pi + 2 \sin^{-1} \left(\frac{b_{z,i}}{b_i} \right) \right] (\mathbf{n}'_i \cdot \hat{\boldsymbol{\sigma}}) \right\}, \quad (\text{B2})$$

where $\mathbf{n}'_i = \mathbf{b}'_i/b'_i$. By the composite unitary transformation $\hat{U} = \hat{u}_1 \otimes \hat{u}_2$ the two-particle inverse Green function can be written as $\hat{\mathcal{G}}(\mathbf{Q}, \mathbf{k}) = \hat{U} \hat{D}(\mathbf{Q}, \mathbf{k}) \hat{U}^\dagger$, where $\hat{D}(\mathbf{Q}, \mathbf{k})$ is identical to (14) but with b_i replaced by \bar{b}_i . The two-particle wave function coefficients can be formed as before (c.f. (9)). The self-consistency condition then reads

$$\frac{1}{|V_0|} = \int \frac{d^2 \mathbf{k}}{(2\pi)^2} s \frac{[s^2 - 2\alpha^2 (\bar{b}^2 + \frac{\bar{B}^2}{4}) - f_1 - f_2]}{d(\mathbf{Q}, \mathbf{k})}, \quad (\text{B3})$$

where $\bar{\mathbf{B}} = \bar{\mathbf{b}}_1 + \bar{\mathbf{b}}_2$ and $\bar{\mathbf{b}} = (\bar{\mathbf{b}}_1 - \bar{\mathbf{b}}_2)/2$, and the denominator is defined as before (c.f. (21)) but with \mathbf{b} and \mathbf{B} replaced by $\bar{\mathbf{b}}$ and $\bar{\mathbf{B}}$, respectively. f_1 and f_2 are given by

$$f_1 = \frac{2\bar{b}_1 \bar{b}_2}{b'_1 b'_2} \left[\alpha^2 \left(\bar{b}^2 - \frac{\bar{B}^2}{4} \right) + H_z^2 \right] \Theta_1 \quad (\text{B4})$$

$$f_2 = -2\bar{b}_1 \bar{b}_2 \Theta_2, \quad (\text{B5})$$

where

$$\Theta_1 = \frac{\sqrt{|\mathbf{H}' + \alpha^2 \bar{\mathbf{b}}|^2 - H_z^2} \sqrt{|\mathbf{H}' - \alpha^2 \bar{\mathbf{b}}|^2 - H_z^2}}{|\mathbf{H}' + \alpha \bar{\mathbf{b}}| |\mathbf{H}' - \alpha \bar{\mathbf{b}}|} \quad (\text{B6})$$

$$\Theta_2 = \frac{H_z^2}{|\mathbf{H}' + \alpha \bar{\mathbf{b}}| |\mathbf{H}' - \alpha \bar{\mathbf{b}}|}. \quad (\text{B7})$$

Appendix C: Obtaining $P(\boldsymbol{\kappa}_1, \boldsymbol{\kappa}_2)$

$P(\boldsymbol{\kappa}_1, \boldsymbol{\kappa}_2)$ is given by the diagonal elements of the density matrix (42). Since the momentum eigenstates $|\mathbf{q}, \boldsymbol{\kappa}\rangle$ are not eigenstates of the Hamiltonian, we must insert a resolution of unity using energy eigenstates. We then obtain

$$\langle \mathbf{q}, \boldsymbol{\kappa} | e^{-\beta \hat{H}} | \mathbf{q}, \boldsymbol{\kappa} \rangle = \sum_n \int_{\mathbf{q}'} \langle \mathbf{q}, \boldsymbol{\kappa} | \psi_n(\mathbf{q}') \rangle \langle \psi_n(\mathbf{q}') | \mathbf{q}, \boldsymbol{\kappa} \rangle e^{-e_n(\mathbf{q}')/\tau}. \quad (\text{C1})$$

At low temperatures, we can safely assume that most of the fermions are in the $n = 0$ bound state. Therefore, we may approximate the above matrix element by

$$\langle \mathbf{q}, \boldsymbol{\kappa} | e^{-\beta \hat{H}} | \mathbf{q}, \boldsymbol{\kappa} \rangle \approx \int_{\mathbf{q}'} \langle \mathbf{q}, \boldsymbol{\kappa} | \psi_0(\mathbf{q}') \rangle \langle \psi_0(\mathbf{q}') | \mathbf{q}, \boldsymbol{\kappa} \rangle e^{-e_0(\mathbf{q}')/\tau}. \quad (\text{C2})$$

Using (3) and (9) we may write (C2) as

$$\langle \mathbf{q}, \boldsymbol{\kappa} | e^{-\beta \hat{H}} | \mathbf{q}, \boldsymbol{\kappa} \rangle \approx |c_{\mathbf{q}}^0|^2 V_0^2 \langle \mathbf{q} | \mathbf{q} \rangle \times \langle 00 | \hat{\mathcal{G}}_0^\dagger(\mathbf{q}, \boldsymbol{\kappa}) \hat{\mathcal{G}}_0(\mathbf{q}, \boldsymbol{\kappa}) | 00 \rangle e^{-e_0(\mathbf{q})/\tau}. \quad (\text{C3})$$

(46) follows directly from this expression.

¹ J.A. Sauls, in *Timing Neutron Stars*, H. Ögelman and E. van den Heuvel eds., (Kluwer, Dordrecht, 1989).
² L. Cooper, *Phys. Rev.* **104**, 1189 (1956).
³ J. Schrieffer, *Theory of Superconductivity*, (Benjamin, New York, 1964).
⁴ S. Giorgini, L.P. Pitaevski and S. Stringari, *Rev. Mod. Phys.* **80**, 1215 (2008).
⁵ E. Tiesinga, A. J. Moerdijk, B. J. Verhaar and H. T. C. Stoof, *Phys. Rev. A* **46**, R1167 (1992).
⁶ E. Tiesinga, B. J. Verhaar and H. T. C. Stoof, *Phys. Rev. A* **47**, 4114 (1993).
⁷ A. J. Moerdijk, B. J. Verhaar and A. Axelsson, *Phys. Rev. A* **51**, 4852 (1995).
⁸ J. M. Vogels, C. C. Tsai, R. S. Freeland, S. J. J. M. F. Kokkelmans, B. J. Verhaar and D. J. Heinzen, *Phys. Rev. A* **56**, R1067 (1997).
⁹ H. M. J. M. Boesten, J. M. Vogels, J. G. C. Tempelaars and B. J. Verhaar, *Phys. Rev. A* **54**, R3726 (1996).

¹⁰ T. Loftus, C. A. Regal, C. Ticknor, J. L. Bohn and D. S. Jin, *Phys. Rev. Lett.* **88**, 173201 (2002).
¹¹ K. M. O'Hara, S. L. Hemmer, M. E. Gehm, S. R. Granade and J. E. Thomas, *Science* **298**, 2179 (2002).
¹² T. Bourdel, J. Cubizolles, L. Khaykovich, K. M. F. Magalhães, S. J. J. M. F. Kokkelmans, G. V. Shlyapnikov and C. Salomon, *Phys. Rev. Lett.* **91**, 020402 (2003).
¹³ S. Jochim, M. Bartenstein, A. Altmeyer, G. Hendl, S. Riedl, C. Chin, J. Hecker Denschlag and R. Grimm, *Science* **302**, 2101 (2003).
¹⁴ M. W. Zwierlein, C. A. Stan, C. H. Schunck, S. M. F. Raupach, A. J. Kerman and W. Ketterle, *Phys. Rev. Lett.* **92**, 120403 (2004).
¹⁵ D. M. Eagles, *Phys. Rev.* **186**, 456 (1969).
¹⁶ A. J. Leggett, in *Modern Trends in the Theory of Condensed Matter*, A. Pekalski and R. Przystawa eds., (Springer-Verlag, Berlin, 1980).
¹⁷ A. J. Leggett, *Quantum Liquids: Bose Condensation and*

- Cooper Pairing in Condensed-Matter Systems*, (Oxford University Press, 2006).
- ¹⁸ M. Randeria, in *Bose-Einstein Condensation*, A. Griffin, D. Snoke and S. Stringari eds., (Cambridge University Press, 1995).
 - ¹⁹ M. Greiner, C. A. Regal and D. S. Jin, *Nature* **426**, 537 (2003).
 - ²⁰ M. W. Zwierlein, C. A. Stan, C. H. Schunck, S. M. F. Raupach, S. Gupta, Z. Hadzibabic and W. Ketterle, *Phys. Rev. Lett.* **91**, 250401 (2003).
 - ²¹ M. Bartenstein, A. Altmeyer, S. Riedl, S. Jochim, C. Chin, J. Hecker-Denschlag and R. Grimm, *Phys. Rev. Lett.* **92**, 120401 (2004).
 - ²² T. Bourdel, L. Khaykovich, J. Cubizolles, J. Zhang, F. Chevy, M. Teichmann, L. Tarruell, S. J. J. M. F. Kokkelmans and C. Salomon, *Phys. Rev. Lett.* **93**, 050401 (2004).
 - ²³ G. B. Partridge, K. E. Strecker, R. I. Kamar, M. W. Jack and R. G. Hulet, *Phys. Rev. Lett.* **95**, 020404 (2005).
 - ²⁴ W. Ketterle and M. W. Zwierlein, *Rivista del Nuovo Cimento* **31**, 247 (2008).
 - ²⁵ I. Bloch, J. Dalibard and W. Zwerger, *Rev. Mod. Phys.* **80**, 885 (2008).
 - ²⁶ D. Jaksch and P. Zoller, *New Journal of Physics* **5**, 56 (2003).
 - ²⁷ K. Osterloh, M. Baig, L. Santos, P. Zoller and M. Lewenstein, *Phys. Rev. Lett.* **95**, 010403 (2005).
 - ²⁸ J. Ruseckas, G. Juzeliūnas, P. Öhberg, and M. Fleischhauer, *Phys. Rev. Lett.* **95**, 010404 (2005).
 - ²⁹ F. Gerbier and J. Dalibard, *New Journal of Physics* **12**, 33007 (2010).
 - ³⁰ T. D. Stanescu, C. Zhang and V. Galitski, *Phys. Rev. Lett.* **99**, 110403 (2007).
 - ³¹ S. L. Zhu, H. Fu, C. J. Wu, S. C. Zhang and L. M. Duan, *Phys. Rev. Lett.* **97**, 240401 (2006).
 - ³² Y.-J. Lin, R. L. Compton, A. R. Perry, W. D. Phillips, J. V. Porto and I. B. Spielman, *Phys. Rev. Lett.* **102**, 130401 (2009).
 - ³³ Y.-J. Lin, R. L. Compton, K. Jimenez-Garcia, J. V. Porto and I. B. Spielman, *Nature* **462**, 628 (2009).
 - ³⁴ Y.-J. Lin, K. Jimenez-Garcia and I. B. Spielman, *Nature* **471**, 83 (2011).
 - ³⁵ S. Das Sarma and A. Pinczuk, eds., *Perspectives in quantum Hall effects: novel quantum liquids in low-dimensional semiconductor structures*, (Wiley, New York, 1997).
 - ³⁶ C. Nayak, S. H. Simon, A. Stern, M. Freedman and S. Das Sarma, *Rev. Mod. Phys.* **80**, 1083 (2008).
 - ³⁷ Z. M. Hasan and C. L. Kane, *Rev. Mod. Phys.* **82**, 3045 (2010).
 - ³⁸ X.-L. Qi and S.-C. Zhang, *Rev. Mod. Phys.* **83**, 1057 (2011).
 - ³⁹ A. V. Chaplik and L. I. Magarill, *Phys. Rev. Lett.* **96**, 126402 (2006).
 - ⁴⁰ E. Cappelluti, C. Grimaldi and F. Marsiglio, *Phys. Rev. Lett.* **98**, 167002 (2007).
 - ⁴¹ H. Zhai, arXiv:1110.6798.
 - ⁴² J. P. Vyasankere and V. B. Shenoy, *Phys. Rev. B* **83**, 094515 (2011).
 - ⁴³ J. P. Vyasankere, S. Zhang and V. B. Shenoy, *Physical Review B* **84**, 014512 (2011).
 - ⁴⁴ M. Iskin, and A. L. Subasi, *Phys. Rev. A* **84**, 043621 (2011); *Phys. Rev. Lett.* **107**, 050402 (2011).
 - ⁴⁵ G. Chen, M. Gong, and C. Zhang, arXiv:1107.2627.
 - ⁴⁶ Z.-Q. Yu and H. Zhai, arXiv:1105.2250.
 - ⁴⁷ M. Sato, Y. Takahashi and S. Fujimoto, *Phys. Rev. Lett.* **103**, 020401 (2009).
 - ⁴⁸ J.-N. Zhang, Y.-H. Chan and L.-M. Duan, arXiv:1110.2241.
 - ⁴⁹ A. Kubasiak, P. Massignan and M. Lewenstein, *Europhys. Lett.* **92**, 46004 (2010).
 - ⁵⁰ K. Seo, L. Han and C. A. R. Sa de Melo, arXiv:1108.4068.
 - ⁵¹ M. Gong, S. Tewari and C. Zhang, arXiv:1105.1796.
 - ⁵² H. Hu, L. Jiang, X.-J. Liu and H. Pu, arXiv:1105.2488.
 - ⁵³ J. P. Vyasankere and V. B. Shenoy, arXiv:1108.4872.
 - ⁵⁴ E. Altman, E. Demler and M. Lukin, *Phys. Rev. A* **70**, 013603 (2004).
 - ⁵⁵ J. D. Koralek, C. P. Weber, J. Orenstein, B. A. Bernevig, S. Zhang, S. Mack and D. D. Awschalom, *Nature* **458**, 610 (2009).
 - ⁵⁶ T. D. Stanescu and V. Galitski, *Phys. Rev. B* **75**, 125307 (2007).
 - ⁵⁷ B. A. Bernevig, J. O. Orenstein, and S. Zhang, *Phys. Rev. Lett.* **97**, 236601 (2006).
 - ⁵⁸ D. S. Petrov, *Phys. Rev. A* **67**, 010703 (2003).
 - ⁵⁹ D. S. Petrov, C. Salomon and G. V. Shlyapnikov, *Phys. Rev. Lett.* **93**, 090404 (2004).
 - ⁶⁰ P. Pieri and G. C. Strinati, *Phys. Rev. Lett.* **96**, 150404 (2006).
 - ⁶¹ I. V. Brodsky, M. Yu. Kagan, A. V. Klaptsov, R. Combescot and X. Leyronas, *Phys. Rev. A* **73**, 032724 (2006).
 - ⁶² E. Taylor, A. Griffin and Y. Ohashi, *Phys. Rev. A* **76**, 023614 (2007).
 - ⁶³ D. L. Campbell, G. Juzeliūnas, and I. B. Spielman, *Phys. Rev. A* **84**, 025602 (2011).